Insights into the evolution from ferromagnetism to antiferromagnetism: A doping-dependent study of $NaCrSi_xGe_{2-x}O_6$ ($0 \leqslant x \leqslant 2$)

W. Tian,[1,*] J.-Q. Yan,[2] and A. I. Kolesnikov[1]

[1]*Neutron Scattering Division, Oak Ridge National Laboratory, Oak Ridge, Tennessee 37831, USA*

[2]*Materials Science and Technology Division, Oak Ridge National Laboratory, Oak Ridge, Tennessee 37831, USA*

(Received 3 January 2019; published 20 February 2019)

$NaCrGe_2O_6$ and $NaCrSi_2O_6$ are isostructural compounds exhibiting different magnetic ground states. $NaCrGe_2O_6$ adopts a ferromagnetic ground state with $Tc = 6$ K, whereas $NaCrSi_2O_6$ orders antiferromagnetically below $T_N = 3.4$ K. Although it has been proposed that the intriguing magnetic behavior in Cr-based pyroxenes involves competition between antiferromagnetic direct exchange and ferromagnetic superexchange interactions, a delicate balance that is sensitive to Cr-Cr distance and local distortion, no spectroscopy study has been done to determine the microscopic interactions in these compounds. To delve deeper into the evolution from ferromagnetism to antiferromagnetism, we performed a doping-dependent study to investigate how the substitution of Ge by Si affects the magnetic properties of $NaCrSi_xGe_{2-x}O_6$ ($x = 0$, 0.5, 1, 1.5, 2). Neutron diffraction and magnetization measurements show that replacing larger Ge with smaller Si simultaneously suppresses the ferromagnetic order. The lattice constants and the unit-cell volume contract, i.e., chemical pressure effect, and the Cr-Cr distance within the chain gradually decreases with increasing Si doping. High-resolution inelastic neutron-scattering studies of the spin waves of $NaCrGe_2O_6$ and $NaCrSi_2O_6$ indicate that replacing Ge with Si has profound effect on the intrachain coupling, whereas it has negligible effect on the interchain couplings. We compare our results, which indicate $NaCrGe_2O_6$ is magnetic quasi-one-dimensional (1D) and $NaCrSi_2O_6$ is three-dimensional (3D), with $LiCr(Si, Ge)_2O_6$, where $LiCrSi_2O_6$ is proposed to be magnetic quasi-1D and $LiCrGe_2O_6$ is 3D, and discuss the different behaviors in magnetic dimensionality crossover in the context of how substituting Ge with Si fine-tunes the relative ratio between the intrachain and interchain couplings that defines the magnetic dimensionality in these materials.

DOI: 10.1103/PhysRevB.99.064427

I. INTRODUCTION

Pyroxenes with chemical formula AMB_2O_6 (where $A =$ Li, Na, or Ca, Mg; $M = 3d$ transition metals with 3+ valence or Mg, Al; $B =$ Si, Ge) are an important family of materials that have been widely studied for decades. The interest in these materials are twofold: (1) The study of silicate pyroxenes is desired for earth sciences as they are major rock-forming minerals found in the Earth's mantle or crust; (2) many pyroxenes are complex magnets, exhibiting intriguing magnetic properties particularly important to fundamental research. As depicted in Fig. 1, the structure of pyroxenes consists of $M^{3+}O_6$ octahedra forming edge-sharing zigzag chains along the c axis and the magnetic interactions between neighboring chains are mediated through BO_4 tetrahedra. The interchain interactions (J_2 and J_3) are considered to be much weaker than the intrachain interaction (J_1) which characterizes pyroxenes as magnetic quasi-one-dimensional (1D). With increasing $3d$ electrons, pyroxenes of various transition-metal ions display a curious evolution of magnetic properties. For instance, $(Li, Na)TiSi_2O_6$ (d^1, $S = 1/2$) exhibit an orbital-assisted spin-Peierls state [1–3]. In the case of $(Li,Na)V(Si, Ge)_2O_6$ (d^2, $S = 1$) [4–6], which in principle can be considered as a physical realization of $S = 1$ Haldane chains, the expected Haldane gap is quenched due to interchain interactions that are large enough to induce magnetic long-range order in the system. Recent studies further reveal that pyroxenes form a new class of multiferroics [7–9]. A magnetoelectric effect has been observed in several Cr-based (d^3, $S = 3/2$) [10,11] and Fe-based (d^5, $S = 5/2$) [12,13] pyroxenes. Moreover, it has been shown that Jahn-Teller distortion plays an important role in the magnetism of $NaMnGe_2O_6$ (d^4, $S = 2$) [14] and $LiNiSi_2O_6$ (d^7, $S = 1/2$) [15], both requiring synthesis under high pressure. Pyroxenes provide a vast playground for exploring the variety of magnetic behaviors emerging from the intricate interplay between spin, charge, orbital, and lattice degrees of freedom.

Cr-based pyroxenes with a $(Li,Na)Cr(Si, Ge)_2O_6$ chemical formula represent a unique group of materials exhibiting fascinating magnetic properties fine-tuned by crystal structure and local distortion that can be attributed to different atom radii on the A site and B site [10,11,16–22]. In these compounds, the electronic configuration of Cr^{3+} is d^3 ($S = 3/2$), resulting in half-filled t_{2g} and empty e_g orbitals. Prior study has shown that the crystal structure is sensitive to the atom radii on the A site: $NaCr(Si, Ge)_2O_6$ crystallizes in a monoclinic unit cell with space group $C2/c$ [11,16], whereas $LiCr(Si, Ge)_2O_6$ [17] adopts a $P2_1/c$ structure at low temperature, indicating that replacing Na (ionic radius $R^{IV}_{Na^{1+}} = 1.02$ Å) with Li (ionic radius $R^{IV}_{Li^{1+}} = 0.76$ Å) reduces the symmetry of the material. Among them, $LiCr(Si, Ge)_2O_6$

*wt6@ornl.gov

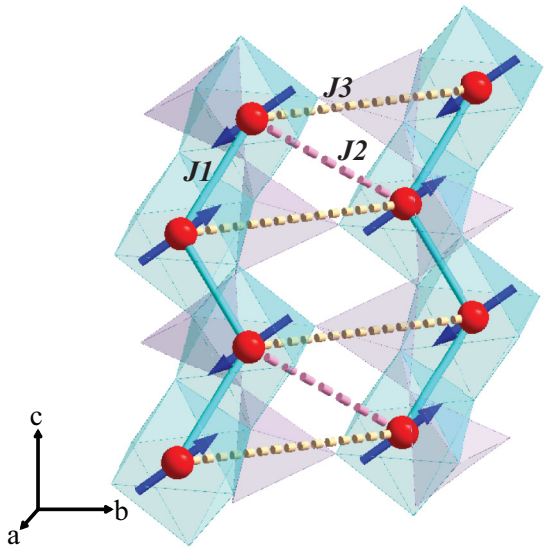

FIG. 1. Schematic view of the $NaCrSi_2O_6$ magnetic structure. Two chains made of CrO_6 octahedra (cyan) and their coupling via SiO_4 tetrahedra (pink) are illustrated. Only the Cr^{3+} (red balls) magnetic ions are shown for clarity. The intrachain (J1) and interchain (J2 and J3) magnetic exchange interactions are labeled.

[10] and $NaCrSi_2O_6$ [11] exhibit a magnetoelectric effect with antiferromagnetic (AFM) ground state at zero field, except for $NaCrGe_2O_6$, which shows a different magnetic behavior. To our knowledge, $NaCrGe_2O_6$ is the only pyroxene with ferromagnetic (FM) order [14]. This compound also has the lowest ordered magnetic moment compared to other Cr-based pyroxenes [18]. The magnetism of $NaCrSi_2O_6$, on the other hand, has been proposed to be at the borderline between AFM and FM, and the system undergoes a magnetic field-induced transition from the AFM state to FM state at 6 T [11]. Given that $NaCrSi_2O_6$ and $NaCrGe_2O_6$ are isostructural, it is appropriate to link their different magnetic ground states to the different atoms at the B site. Although it has been proposed that the complex magnetic behavior in $NaCr(Si, Ge)_2O_6$ involves competition between AFM and FM contributions that is sensitive to local distortion, orbital occupancy, and orbital orientation [19], no spectroscopy study has been carried out to determine the microscopic interactions. In order to provide further information concerning the microscopic origin of the different magnetic ground states, we performed a doping-dependent study using neutron-scattering and magnetization measurements to examine how the substitution of larger Ge^{4+} (ionic radius $R^{IV}_{Ge^{4+}} = 0.39$ Å) with smaller Si^{4+} (ionic radius $R^{IV}_{Si^{4+}} = 0.26$ Å) affects the evolution from ferromagnetism to antiferromagnetism in $NaCrSi_xGe_{2-x}O_6$ ($x = 0, 0.5, 1, 1.5, 2$).

II. EXPERIMENTAL METHODS

Polycrystalline $NaCrSi_xGe_{2-x}O_6$ samples were synthesized by a solid-state reaction method, where $x = 0$, 0.5, 1, 1.5, and 2 represent the nominal compositions. High-purity Na_2CO_3, Cr_2O_3, and SiO_2/GeO_2 were mixed in the appropriate stoichiometric ratios and placed in high-density aluminum oxide crucibles. The materials were fired in air for 2 days at 1000 °C–1050 °C with intermediate grindings. Powder x-ray diffraction measurements confirmed the obtained samples are of high quality and single phase. The magnetic susceptibility and magnetization were measured using a superconducting quantum interference device (SQUID) magnetometer down to 2 K. Neutron diffraction measurements were performed using the HB-1A triple-axis spectrometer located at the High Flux Isotope Reactor (HFIR) at the Oak Ridge National Laboratory (ORNL). The powder samples, ~5 grams each, were loaded in standard vanadium can and diffraction patterns were collected at selected temperatures using an orange cryostat. Rietveld refinements of the neutron data were carried out using the FULLPROF program [23]. Inelastic neutron-scattering measurements of $NaCrSi_2O_6$ and $NaCrGe_2O_6$ were performed using the SEQUOIA [24] direct geometry time-of-flight chopper spectrometer at the Spallation Neutron Source at ORNL. Both samples were loaded in flat-plate aluminum cell to completely cover the 5×5 cm beam and measured using an orange cryostat. The experiments were carried out using an incident energy of $E_i = 8$ meV with the Fermi chopper spins at 180 Hz and T_0 chopper spins at 60 Hz, providing a fine energy resolution (FWHM) of 0.2 meV at the elastic line. Data were collected at $T = 1.8$ and 10 K, and normalized to vanadium to remove variation in detector efficiency. Background data from an empty aluminum can were subtracted from the signal.

III. RESULTS AND DISCUSSIONS

Figure 2 shows the magnetization and magnetic susceptibility results of $NaCrSi_xGe_{2-x}O_6$. Our data for both undoped samples are in good agreement with previous reports that confirm the FM order in $NaCrGe_2O_6$ at $Tc = 6$ K [16] and AFM order in $NaCrSi_2O_6$ at $T_N = 3.4$ K [11,18]. The magnetization of $NaCrGe_2O_6$ saturates very rapidly, typical for material with FM order. The doped compounds ($x = 0.5$, 1, and 1.5) exhibit similar behavior, indicating FM ground state in these materials as well. The saturation field gradually increases with increasing Si doping, suggesting that substituting Ge by Si simultaneously suppresses the FM order. This is also supported by the magnetic susceptibility data [Fig. 2(b)], which shows the FM ordering temperature T_c decreases with increasing Si doping. The trend is further illustrated in the inverse magnetic susceptibility [Fig. 2(b), inset]. The high-temperature susceptibility follows Curie-Weiss behavior, with a similar slope for all five compounds, indicating very little doping dependence. Fitting the susceptibility data between 100 and 300 K to Curie-Weiss law results in an effective paramagnetic moment $\mu_{\text{eff}} \approx 3.7\ \mu_B$, which is close to the theoretical value of 3.87 μ_B for a free Cr^{3+} ion. The obtained Curie temperatures $\theta_{cw} = 11.85, 8.2, 2.45, 0.92$, and -0.25 K for $x = 0$, 0.5, 1, 1.5, and 2 suggest FM ($x = 0$, 0.5, 1, and 1.5) and AFM ($x = 2$) ground states in these materials. The Curie-Weiss temperature decreases with increasing Si doping and switches from a positive value for $x = 1.5$ to a negative value for $x = 2$. This suggests that a critical doping x_c may exist in $NaCrSi_xGe_{2-x}O_6$, at which the magnetic order could be completely suppressed with the material being FM for $x < x_c$ and AFM for $x > x_c$. In fact, the low-temperature inverse susceptibility of the $x = 1.5$ sample is close to linear, suggesting it is close to x_c. However, mapping out the doping-dependent phase diagram is a tremendous amount of work that

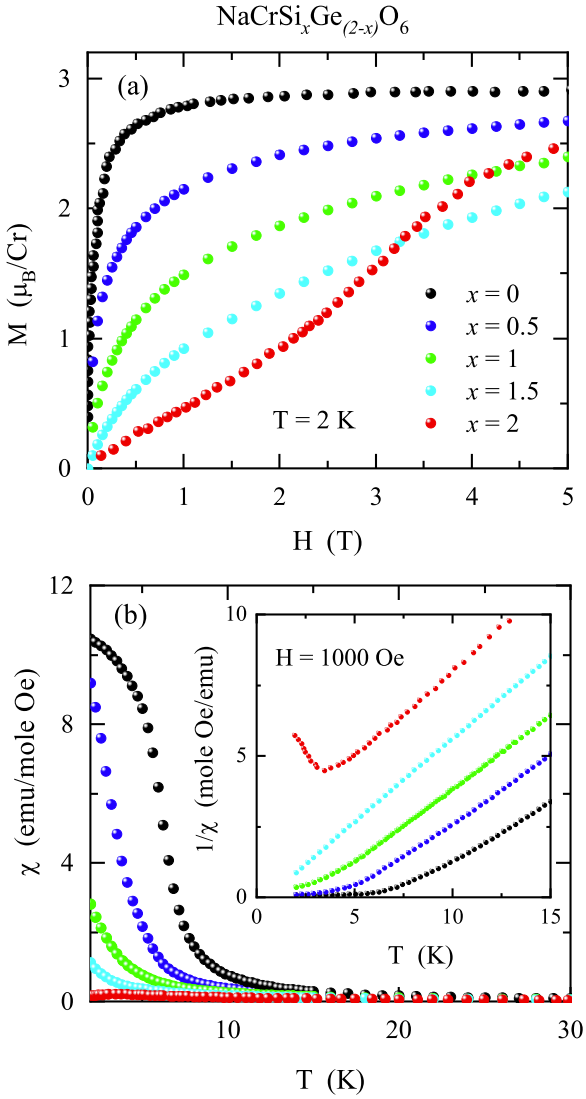

FIG. 2. (a) The field dependence of magnetization measured at 2 K and (b) temperature dependence of magnetic susceptibility measure with $H = 1000$ Oe for $NaCrSi_xGe_{2-x}O_6$. The low-temperature region of the inverse susceptibility is enlarged in the inset.

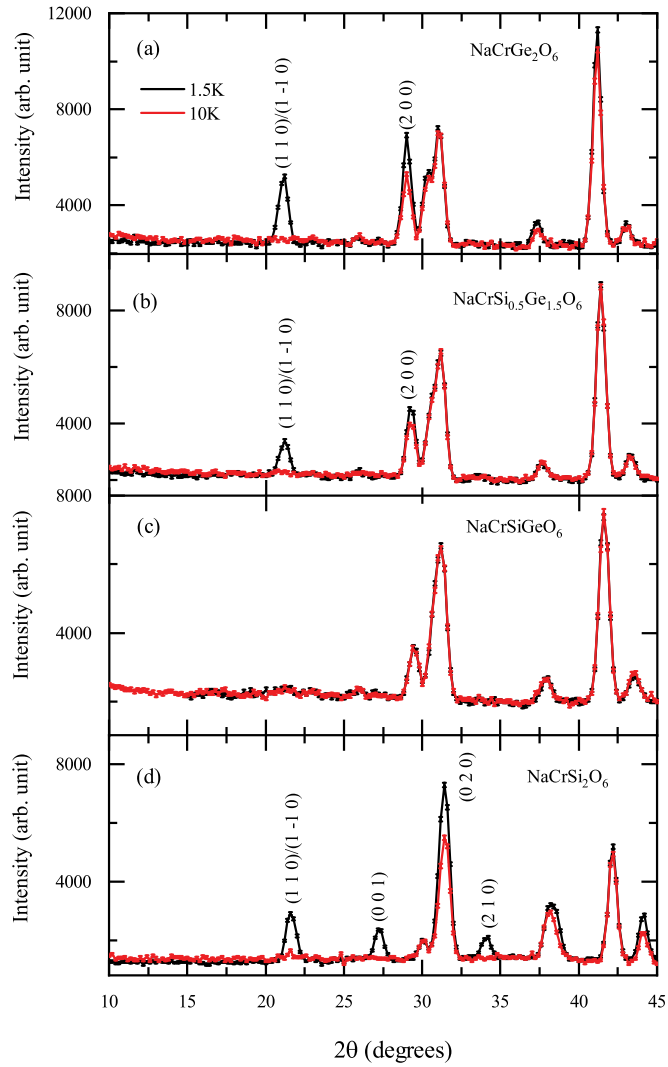

FIG. 3. Neutron powder diffraction pattern of $NaCrSi_xGe_{2-x}O_6$ between $10^\circ \leqslant 2\theta \leqslant 45^\circ$ measured at 1.5 and 10 K: (a) $x = 0$, (b) $x = 0.5$, (c) $x = 1$, and (d) $x = 2$.

is beyond the scope of this study. The results presented here can serve as the groundwork for further investigations.

To provide further information on the magnetic orders in doped samples, we performed neutron powder diffraction experiments to compare the magnetic structures of $NaCrSi_xGe_{2-x}O_6$ for $x = 0$, 0.5, 1, and 2. The low-angle data between $10^\circ \leqslant 2\theta \leqslant 45^\circ$ are shown in Fig. 3 to highlight the observed magnetic peaks at 1.5 K. At 10 K, similar diffraction patterns collected over the range of $10^\circ \leqslant 2\theta \leqslant 120^\circ$ were observed in all samples, indicating no doping-induced structural transition. This is as expected, since both $NaCrGe_2O_6$ and $NaCrSi_2O_6$ have been shown to crystallize in the same structure. At 1.5 K, additional magnetic scattering is observed in Figs. 3(a), 3(b) and 3(d) corresponding to magnetic long-range order transitions. $NaCrGe_2O_6$ [Fig. 3(a)] and $NaCrSi_{0.5}Ge_{1.5}O_6$ [Fig. 3(b)] display similar diffraction patterns, indicating they adopt the same magnetic structure. The data for $NaCrSi_2O_6$ clearly shows that it has different magnetic structure, evidenced by the extra magnetic peaks [(0 0 1) and (2 1 0) in Fig. 3(d)]. No magnetic signal was observed in $NaCrSiGeO_6$ [Fig. 3(c)] down to 1.5 K, which is presumably caused by Tc being reduced to below 1.5 K. The observed magnetic peaks in the $x = 0$, 0.5, and 2 samples can be indexed by a propagation vector of $k = 0$, commensurate with the lattice. The 10 K data can be well refined with a $C2/c$ space group, and the Rietveld refinements of the 1.5 K data using FULLPROF [23] confirm the magnetic space group is $C2'/c'$ for $NaCrGe_2O_6$ and $NaCrSi_{0.5}Ge_{1.5}O_6$, with moments aligned along the c axis and $C - 1'$ for $NaCrSi_2O_6$ with moments lying in the ac plane in good agreement with previous reports [11,16]. The order parameter measurements (Fig. 4) determine the transition temperature $Tc = 6$, 4.5, and 3.4 K for $NaCrSi_xGe_{2-x}O_6$ with $x = 0$, 0.5, and 2, respectively, in excellent agreement with the susceptibility data. We summarize the doping dependence of lattice parameters, magnetic ordering temperature, and the Cr-Cr distance within the chain in Table I. It shows that the lattice constants and the unit-cell volume contract with increased Si doping, i.e., chemical

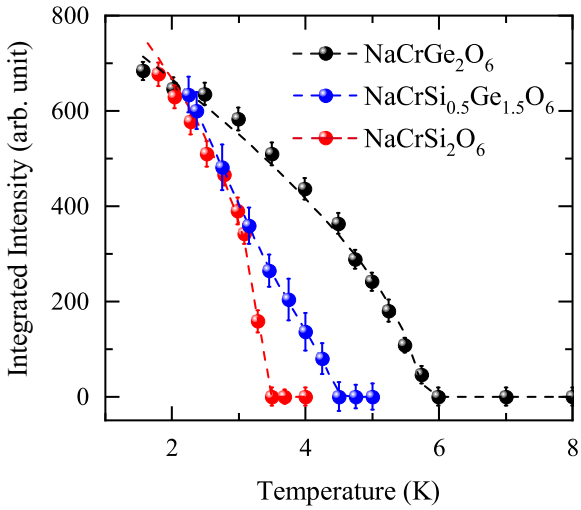

FIG. 4. Order parameter of $NaCrSi_xGe_{2-x}O_6$: temperature dependence of the integrated intensity of (1 1 0) magnetic peak for $x = 0$, 0.5, and 2.

pressure effect. Consequently, the Cr-Cr distance within the chain also decreases with increasing Si doping. Overall, the structural refinement of neutron powder diffraction data at 10 K reveals that the lattice evolves smoothly going from Ge to Si in $NaCrSi_xGe_{2-x}O_6$.

To gain insights into the microscopic interactions, we performed inelastic neutron-scattering (INS) experiments to measure the spin dynamics of undoped compounds. The low-energy magnon spectra measured in the ordered phase and the powder-averaged spin-wave dispersion calculated within linear spin-wave theory are shown in Figs. 5 and 6 for $NaCrGe_2O_6$ and $NaCrSi_2O_6$, respectively. Excitation with energy transfer centered at approximately 2.6 meV in $NaCrGe_2O_6$ [Fig. 5(a)] and 0.5 meV in $NaCrSi_2O_6$ [Fig. 6(a)] are observed. The excitation disappears at temperatures above T_N (Fig. 7), clarifying they are magnetic in origin. For both compounds, the spin-wave spectrum is gapless within the ~0.2 meV instrumental energy resolution. The excitation arises from the magnetic zone centers, consistent with $k = 0$ wave-vector and the spin-wave theory.

We analyze the measured magnetic spectra using linear spin-wave theory and take into account magnetic exchange interactions up to third nearest-neighbor (J_1, J_2, and J_3) as illustrated in Fig. 1. The Heisenberg spin Hamiltonian can be expressed in the following form:

$$\mathcal{H} = \sum_{i,j} J_{ij} \mathbf{S}_i \cdot \mathbf{S}_j, \quad (1)$$

where negative and positive J values correspond to ferromagnetic and antiferromagnetic interactions, respectively. SPINW software [25] was used to compute the spin-wave dispersion in Eq. (1), and the exchange coupling constants were determined by comparing the measured spectrum to powder-averaged scattering intensity calculated within linear spin-wave theory. The calculated scattering intensity was convolved with a Gaussian function, the peak width (FWHM) of which was fixed to 0.2 meV, corresponding to the instrumental energy resolution at elastic line.

Figure 5 summarizes the experimental and simulated results for $NaCrGe_2O_6$. The fitted spectra by including the intrachain interaction J_1 only, the most dominant term in the Hamiltonian, is plotted in Fig. 5(b). It shows that the simple chain model with $J_1 = -0.45 \pm 0.01$ (meV) captures the main feature of the magnetic spectrum. In Figs. 5(c) and 5(d) we plot the simulated results by including both $J_1 = -0.43 \pm 0.01$ meV and $J_2 = -0.03 \pm 0.005$ meV, and all three interactions ($J_1 = -0.41 \pm 0.01$ meV, $J_2 = -0.03 \pm 0.005$ meV, $J_3 = -0.02 \pm 0.005$ meV) in the fitting. It shows that adding interchain couplings introduce additional scattering between 0.5 and 1 $Å^{-1}$ in Q range and 1–2.5 meV in energy transfer. In particular, it improves the agreement between the experimental and simulated spectrum in the low-energy region below $Q = 0.5$ $Å^{-1}$. Figure 6 compares the measured low-temperature spectra with simulated fitting results for $NaCrSi_2O_6$. The fitting results indicate that including two terms ($J_1 = 0.12 \pm 0.02$ meV, $J_2 = 0.02 \pm 0.01$ meV) in the Hamiltonian produces the key feature of the spectrum [Fig. 6(b)]. Adding J_3 [Fig. 6(c)], $J_1 = 0.09 \pm 0.02$ meV, $J_2 = 0.03 \pm 0.01$ meV, $J_3 = -0.02 \pm 0.01$ meV) further improves the fitting result. The enhanced intensity at around $Q = 0.4$ $Å^{-1}$ and the kink in the spectrum at around Q = 1.25 $Å^{-1}$ agree notably better with the measurement result. The spin-wave analysis suggests that for both compounds J_3 is necessary in order to fully account for the magnetic spectrum.

The obtained intrachain coupling constants, $J_1 = -0.41$ meV (~ 4.8 K) for $NaCrGe_2O_6$ and $J_1 = 0.09$ meV (~1 K) for $NaCrSi_2O_6$, are in good agreement with the LSDA + U calculation results in Ref. [19] in which J_1 is estimated to be 5.2 and 0.8 K for $NaCrGe_2O_6$ and $NaCrSi_2O_6$, respectively. The INS results suggest that $NaCrGe_2O_6$ is magnetic quasi-1D with a ratio of $J_1/J_2 \approx 14$ between intrachain and interchain interactions, whereas $NaCrSi_2O_6$ is close to three-dimensional (3D) with $J_1/J_2 \approx 3$. Furthermore, the INS results indicate that although replacing Si with Ge has a profound effect on J_1, the intrachain coupling, it has a negligible effect on the interchain couplings due to the

TABLE I. Doping dependence of crystal structure and magnetic properties of $NaCrSi_xGe_{2-x}O_6$. T_c and $D_{Cr\text{-}Cr}$ represent the magnetic ordering temperature and the distance between Cr-Cr magnetic ions along the chain direction, respectively.

Doping x	a (Å)	b (Å)	c (Å)	β	T_c (K)	$D_{Cr\text{-}Cr}$
0	9.907(2)	8.833(1)	5.454(1)	107.452(10)	6	3.1912(4)
0.5	9.825(1)	8.814(2)	5.405(2)	107.444(25)	4.5	3.1613(9)
1	9.733(4)	8.766(5)	5.365 (2)	107.441(15)		3.1352(10)
2	9.567(2)	8.695(2)	5.263(1)	107.431(29)	3.4	3.0797(12)

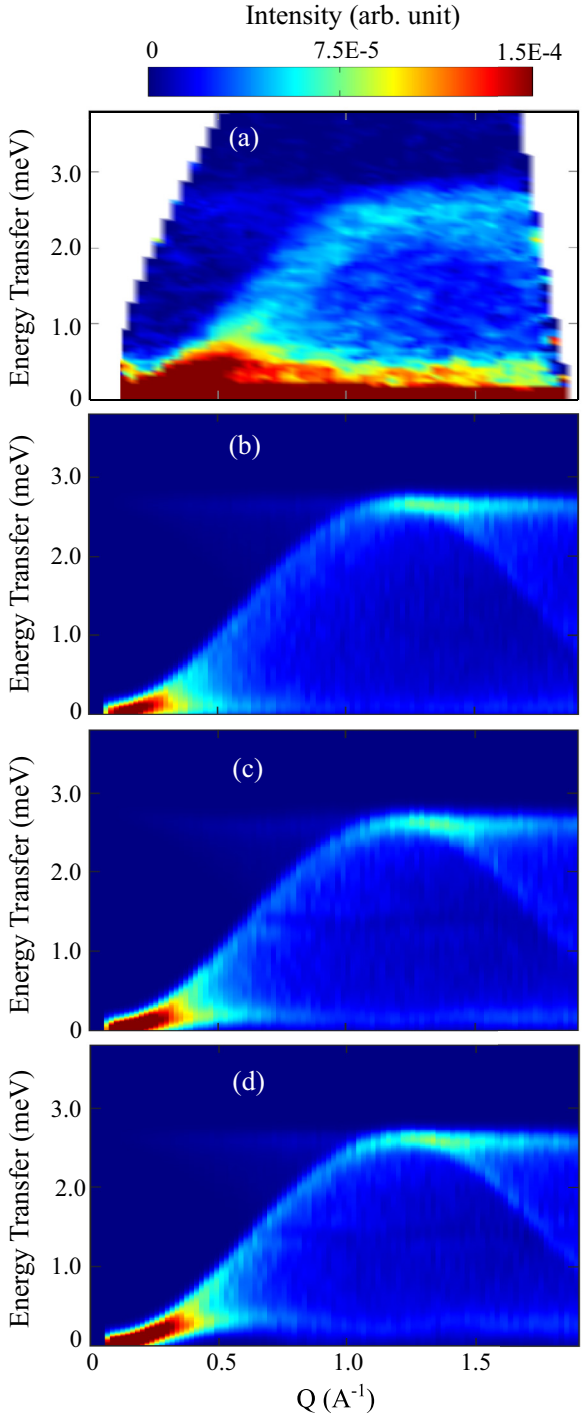

FIG. 5. (a) Low-energy magnet excitation spectrum of $NaCrGe_2O_6$ measured using the SEQUOIA instrument at 1.8 K. Simulated scattering intensity including (b) $J_1 = -0.45 \pm 0.01$ meV; (c) $J_1 = -0.43 \pm 0.01$ meV and $J_2 = -0.03 \pm 0.005$ meV; (d) $J_1 = -0.41 \pm 0.01$ meV, $J_2 = -0.03 \pm 0.005$ meV, and $J_3 = -0.02 \pm 0.005$ meV in Eq. (1).

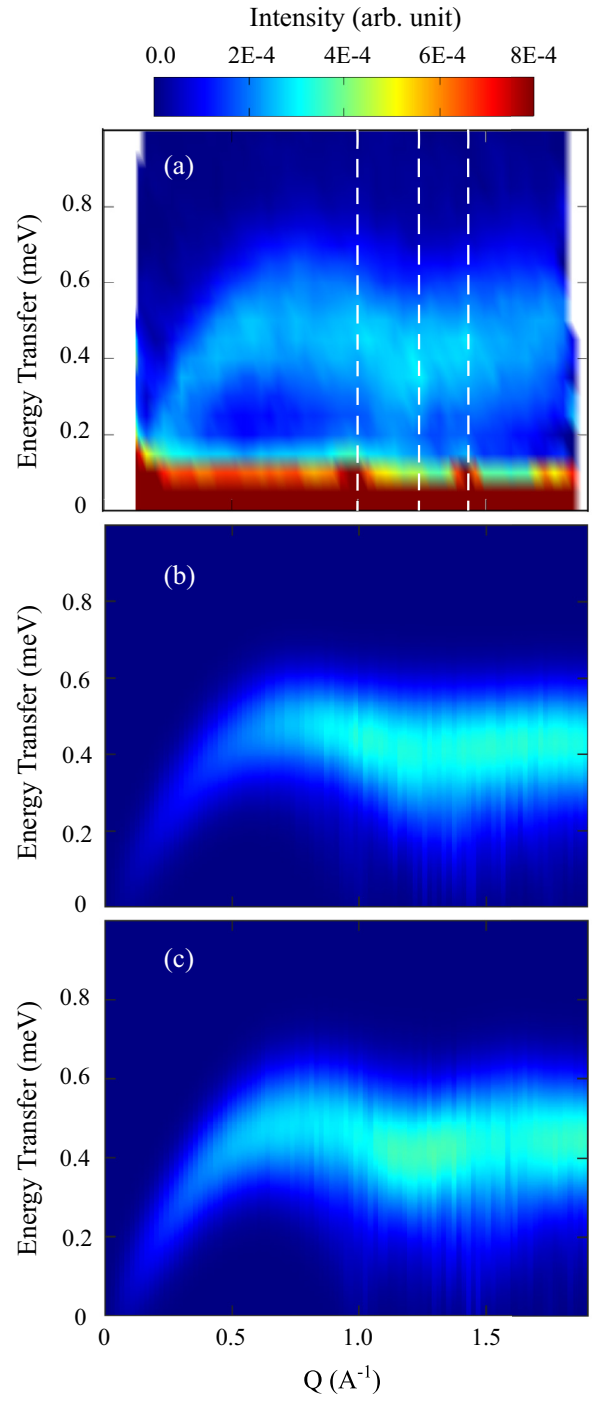

FIG. 6. (a) Low-energy magnet excitation spectrum of $NaCrSi_2O_6$ measured using the SEQUOIA instrument at 1.8 K. The dashed lines denote the Q values corresponding to (1 1 0), (0 0 1), and (0 2 0) magnetic peaks. Simulated scattering intensity including (b) $J_1 = 0.12 \pm 0.02$ meV and $J_2 = 0.05 \pm 0.01$ meV; (c) $J_1 = 0.09 \pm 0.02$ meV, $J_2 = 0.03 \pm 0.01$ meV, and J3 = -0.02 ± 0.01 meV in Eq. (1).

larger Cr-Cr distances ($D_{\text{Cr-Cr}} \approx 5.6$ and 6.8Å for J_2 and J_3, respectively) in comparison with the Cr-Cr distance within the chain ($D_{\text{Cr-Cr}} \approx 3.1$Å for J_1). Similar behavior is also reported in $LiCr(Ge, Si)_2O_6$ [17]. This observation suggests that the different magnetic ground state in $NaCr(Si, Ge)_2O_6$ is mainly controlled by J_1.

It is interesting to compare our $NaCr(Ge, Si)_2O_6$ results with $LiCr(Ge, Si)_2O_6$. In Fig. 8 we summarize the doping dependence of $D_{\text{Cr-Cr}}$ along the chain direction in $NaCrSi_xGe_{2-x}O_6$ and $LiCr(Ge, Si)_2O_6$ and the magnetic ground state and magnetic dimensionality of undoped

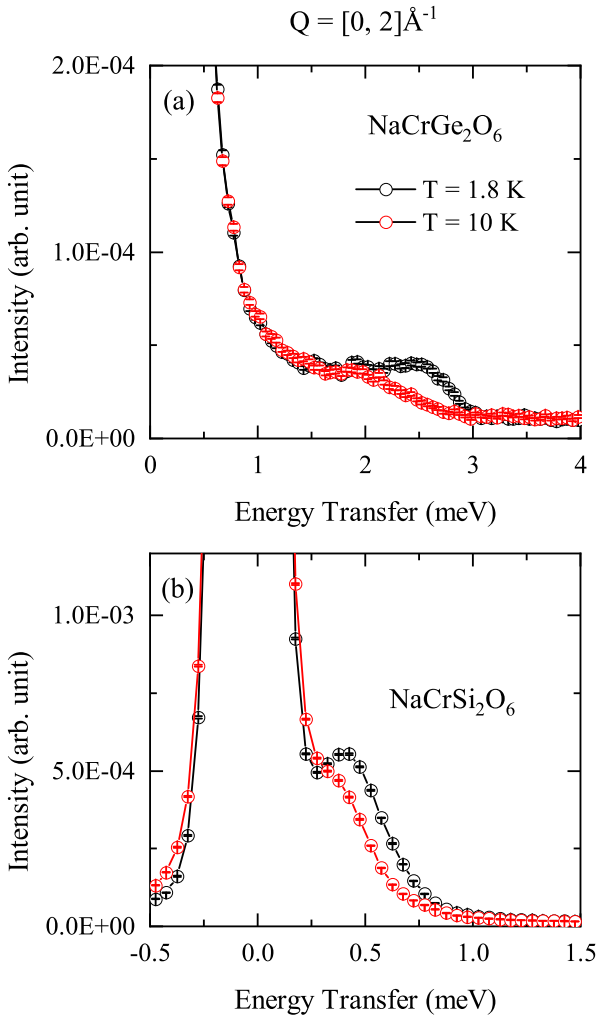

FIG. 7. Intensity vs energy transfer integrated between $Q = 0$ and 2 Å^{-1} for $T = 1.8$ and 10 K indicate the ~2.6 meV and ~0.5 meV magnetic excitation observed in (a) $NaCrGe_2O_6$ and (b) $NaCrSi_2O_6$, respectively.

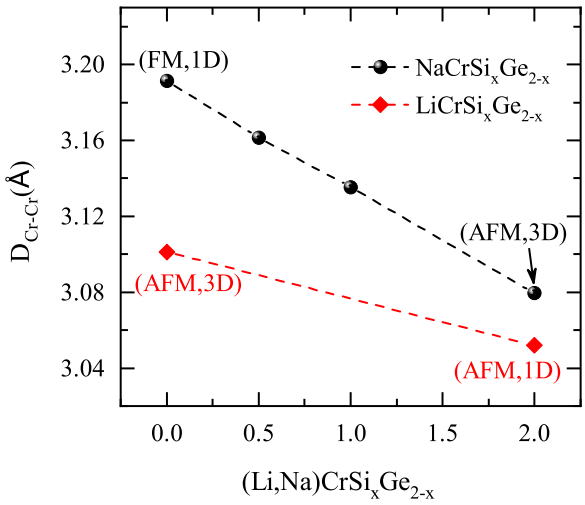

FIG. 8. Doping dependence of $D_{Cr\text{-}Cr}$ for $NaCrSi_xGe_{2-x}O_6$ from this study and $LiCrSi_xGe_{2-x}O_6$ from Ref. [10]. The magnetic ground state and the magnetic dimensionality of the end compounds are labeled.

compounds. In both cases, the substitution of Si by Ge induces magnetic dimensionality crossover. It has been proposed that $LiCrSi_2O_6$ is magnetic quasi-1D and $LiCrGe_2O_6$ is 3D [17]. However, this process is reversed in $NaCr(Ge, Si)_2O_6$. Our results indicate that $NaCrGe_2O_6$ is quasi-1D and $NaCrSi_2O_6$ is 3D. Such a contrast opens a question about what causes the different behavior in magnetic dimensionality crossover given that replacing Si with Ge increases the Cr-Cr distance in both $NaCr(Ge, Si)_2O_6$ and $LiCr(Ge, Si)_2O_6$. In the following, we will discuss that such different behavior may be explained in the context of how substituting Ge with Si fine-tunes the J_1/J_2 ratio, which is used to characterize the dimensionality of a material.

Previous DFT studies [19] reveal that in Cr-based pyroxenes, the intrachain interaction J_1 includes contributions from AFM $t_{2g} \leftrightarrow t_{2g}$ direct exchange and FM half-filled $t_{2g} \leftrightarrow$ empty e_g superexchange interactions. The AFM and FM exchange interactions compete with each other, and the Cr-Cr distance is the key parameter controlling J_1. J_1 is AFM at short Cr-Cr distance due to a strong AFM direct exchange interaction that is dominant, whereas J_1 is FM at larger Cr-Cr distance because the AFM interaction reduces more rapidly than the FM interaction and the superexchange interaction becomes dominant. In other words, the system may be characterized as magnetic quasi-1D with AFM order at shorter Cr-Cr distance and FM order at larger Cr-Cr distance, assuming the interchain couplings are much weaker. In the intermediate Cr-Cr distance, the strength of J_1 is reduced when AFM-FM contributions compensate each other. Hence, we expect the weakened J_1 makes the system less one-dimensional. Among the four $(Li,Na)Cr(Ge, Si)_2O_6$ compounds, $LiCrSi_2O_6$ ($D_{Cr\text{-}Cr}$ = 3.052 Å, Ref. [17]) and $NaCrGe_2O_6$ ($D_{Cr\text{-}Cr}$ = 3.19 Å, this study) have the shortest and largest Cr-Cr distances and have been identified as AFM and FM quasi-1D, respectively. Comparing with $LiCrSi_2O_6$, the Cr-Cr distance is larger in $LiCrGe_2O_6$, which reduces J_1, making the material 3D, while in the case of $NaCrSi_2O_6$, the shorter Cr-Cr distance enhances the AFM exchange interaction that competes with FM contribution. J_1 is significantly reduced ($J_1 = -0.09$ meV), placing this material at the borderline between AFM and FM with an AFM ground state.

IV. SUMMARY

In summary, neutron scattering and magnetization are used to investigate the evolution from ferromagnetism to antiferromagnetism in $NaCrSi_xGe_{2-x}O_6$. Our doping-dependent study shows that substitution of Ge by Si simultaneously suppresses the ferromagnetic order. The Cr-Cr distance also decreases gradually with Si doping due to a steric effect. Spin-wave studies of $NaCrGe_2O_6$ and $NaCrSi_2O_6$ by high-resolution INS reveal that replacing Ge with Si has a profound effect on the intrachain coupling, whereas it has a negligible effect on the interchain couplings. This implies that the Cr-Cr distance is critical to the magnetic properties in $NaCr(Si, Ge)_2O_6$. Replacing larger Ge with smaller Si fine-tunes the delicate balance between AFM direct exchange and FM superexchange contributions that give rise to the different magnetic ground states and magnetic dimensionality crossover. Our data also suggest that a critical doping x_c may exist

in $NaCrSi_xGe_{2-x}O_6$ at which the magnetic order could be completely suppressed, requiring further investigation.

The Department of Energy will provide public access to these results of federally sponsored research in accordance with the DOE Public Access Plan [26].

ACKNOWLEDGMENTS

The neutron-scattering research at the High Flux Isotope Reactor and Spallation Neutron Source, Oak Ridge National Laboratory, was sponsored by the Scientific User Facilities Division, Office of Basic Energy Sciences, U.S. Department of Energy. J.Q.Y. is supported by the U.S. Department of Energy, Office of Science, Basic Energy Sciences, Materials Sciences and Engineering Division. ORNL is managed by UT-Battelle, LLC, under Contract No. DE-AC05-00OR22725 with the U.S. Department of Energy. The U.S. Government retains, and the publisher, by accepting the article for publication, acknowledges that the U.S. Government retains a nonexclusive, paid-up, irrevocable, worldwide license to publish or reproduce the published form of this manuscript, or allow others to do so, for U.S. Government purposes.

[1] M. Isobe, E. Ninomiya, A. N. Vasil'ev, and Y. Ueda, J. Phys. Soc. Jpn. **71**, 1423 (2002).
[2] M. J. Konstantinovic, J. van den Brink, Z. V. Popovic, V. V. Moshchalkov, M. Isobe, and Y. Ueda, Phys. Rev. B, **69**, 020409(R) (2004).
[3] T. Hikihara and Y. Motome, Phys. Rev. B **70**, 214404 (2004).
[4] M. D. Lumsden, G. E. Granroth, D. Mandrus, S. E. Nagler, J. R. Thompson, J. P. Castellan, and B. D. Gaulin, Phys. Rev. B **62**, 9244(R) (2000).
[5] B. Pedrini, S. Wessel, J. L. Gavilano, H. R. Ott, S. M. Kazakov, and J. Karpinski, Eur. Phys. J. B **55**, 219 (2007).
[6] P. Millet, F. Mila, F. C. Zhang, M. Mambrini, A. B. Van Oosten, V. A. Pashchenko, A. Sulpice, and A. Stepanov, Phys. Rev. Lett. **83**, 4176 (1999).
[7] M. Fiebig, J. Phys. D: Appl. Phys. **38**, R123 (2005).
[8] S. Jodlauk, P. Becker, J. A. Mydosh, D. I. Khomskii, T. Lorenz, S. V. Streltsov, D. C. Hezel, and L. Bohat, J. Phys.: Condens. Matter **19**, 432201 (2007).
[9] L. Ding, C. V. Colin, C. Darie, and P. Bordet, J. Mater. Chem. C **4**, 4236 (2016).
[10] G. Nénert, M. Isobe, I. Kim, C. Ritter, C. V. Colin, A. N. Vasiliev, K. H. Kim, and Y. Ueda, Phys. Rev. B **82**, 024429 (2010).
[11] G. Nénert, I. Kim, M. Isobe, C. Ritter, A. N. Vasiliev, K. H. Kim, and Y. Ueda, Phys. Rev. B **81**, 184408 (2010).
[12] I. Kim, B.-G. Jeon, D. Patil, S. Patil, G. Nenert, and K. H. Kim, J. Phys.: Condens. Matter **24**, 306001 (2012).
[13] G. J. Redhammer, A. Senyshyn, S. Lebernegg, G. Tippelt, E. Dachs, and G. Roth, Phys. Chem. Miner. **44**, 669 (2017).
[14] J. Cheng, W. Tian, J. Zhou, Y. M. Lynch, H. Steinfink, A. Manthiram, A. F. May, V. O. Garlea, J. C. Neuefeind, and J.-Q. Yan, J. Am. Chem. Soc. **135**, 2776 (2013).
[15] M. Tribaudino, G. Bromiley, H. Ohashi, and F. Nestola, Phys. Chem. Miner. **36**, 527 (2009).
[16] G. Nenert, C. Ritter, M. Isobe, O. Isnard, A. N. Vasiliev, and Y. Ueda, Phys. Rev. B **80**, 024402 (2009).
[17] O. Janson, G. Nenert, M. Isobe, Y. Skourski, Y. Ueda, H. Rosner, and A. A. Tsirlin, Phys. Rev. B **90**, 214424 (2014).
[18] A. N. Vasiliev, O. L. Ignatchik, A. N. Sokolov, Z. Hiroi, M. Isobe, and Y. Ueda, Phys. Rev. B **72**, 012412 (2005).
[19] S. V. Streltsov and D. I. Khomskii, Phys. Rev. B **77**, 064405 (2008).
[20] G. Nenert, M. Isobe, C. Ritter, O. Isnard, A. N. Vasiliev, and Y. Ueda, Phys. Rev. B **79**, 064416 (2009).
[21] A. N. Vasil'ev, O. L. Ignatchik, A. N. Sokolov, Z. Hiroi, M. Isobe, and Y. Ueda, JETP Lett. **78**, 551 (2003).
[22] G. J. Redhammer, G. Roth, and G. Amthauer, Acta Crystallogr., Sect. C: Cryst. Struct. Commun. **64**, I97 (2008).
[23] J. Rodriguez-Carvajal, Physica B **192**, 55 (1993).
[24] G. E. Granroth, A. I. Kolesnikov, T. E. Sherline, J. P. Clancy, K. A. Ross, J. P. C. Ruff, B. D. Gaulin, and S. E. Nagler, J. Phys.: Conf. Ser. **251**, 12058 (2010).
[25] S. Toth and B. Lake, J. Phys.: Condens. Matter **27**, 166002 (2015).
[26] http://energy.gov/downloads/doepublic-access-plan.